Dalton Transactions

PAPER

Cite this: *Dalton Trans.*, 2017, **46**, 1567

The binuclear dual emitter [Br(CO)$_3$Re(P···N)(N···P)Re(CO)$_3$Br] (P···N): 3-chloro-6-(4-diphenylphosphinyl)butoxypyridazine, a new bridging *P,N*-bidentate ligand resulting from the ring opening of tetrahydrofuran†‡

Marianela Saldías,[a] Jorge Manzur,[b] Rodrigo E. Palacios,[c] María L. Gómez,[c] Julio De La Fuente,[d] Germán Günther,[d] Nancy Pizarro[a] and Andrés Vega*[a,e]

Received 31st October 2016,
Accepted 16th December 2016

DOI: 10.1039/c6dt04158b

rsc.li/dalton

Lithium diphenylphosphide unexpectedly provokes the ring-opening of tetrahydrofuran (THF) and by reaction with 3,6-dichloropyridazine leads to the formation of the ligand 3-chloro-6-(4-diphenylphosphinyl)butoxypyridazine (**P···N**), which was isolated. The reaction of this ligand with the (Re(CO)$_3$(THF)Br)$_2$ dimer yields the novel complex [Br(CO)$_3$Re(μ-3-chloro-6-(4-diphenylphosphinyl)butoxypyridazine)$_2$Re(CO)$_3$Br] (**BrRe(P···N)(N···P)ReBr**), which was crystallized in the form of a chloroform solvate, ($C_{46}H_{40}Br_2Cl_2N_4O_8P_2Re_2$)·($CHCl_3$). The monoclinic crystal ($P2_1/n$) displays a bimetallic cage structure with a symmetry inversion centre in the middle of the rhenium to rhenium line. The molecule shows two oxidation signals occurring at +1.50 V and +1.76 V which were assigned to the Re^{I}/Re^{II} and Re^{II}/Re^{III} metal-centered couples, respectively, while signals observed at –1.38 V and –1.68 V were assigned to ligand centered reductions. Experimental and DFT/TDDFT results indicate that the UV-Vis absorption maximum of **BrRe(P···N)(N···P)ReBr** occurring near 380 nm displays a metal to ligand charge transfer (MLCT) character, which is consistent with CV results. Upon excitation at this wavelength, a weak emission ($\Phi_{em} < 1 \times 10^{-3}$) is observed around 580 nm (in dichloromethane) which decays with two distinct lifetimes τ_1 and τ_2 of 24 and 4.7 ns, respectively. The prevalence of non-radiative deactivation pathways is consistent with efficient internal conversion induced by the high conformational flexibility of the **P···N** ligand's long carbon chain. Measurements in a frozen solvent at 77 K, where vibrational deactivation is hindered, show intense emission associated with the ^{3}MLCT state. These results demonstrate that **BrRe(P···N)(N···P)ReBr** preserves the dual emitting nature previously reported for the mononuclear complex **RePNBr**, with emission associated with π^*_{phenyl} and $\pi^*_{pyridazine}$ states.

[a]*Universidad Andres Bello, Facultad de Ciencias Exactas, Departamento de Ciencias Químicas. Quillota 980, Viña del Mar, Chile. E-mail: andresvega@unab.cl*
[b]*Universidad De Chile, Facultad de Ciencias Físicas y Matemáticas, Departamento de Ciencias de los Materiales, Av. Tupper 2460, Santiago, Chile*
[c]*Universidad Nacional de Rio Cuarto y CONICET, Facultad de Ciencias Exactas Fisicoquímicas y Naturales, Departamento de Química, Campus Universitario, 5800 Río Cuarto, Córdoba, Argentina*
[d]*Universidad De Chile, Facultad de Ciencias Químicas y Farmacéuticas, Departamento de Química Orgánica y Fisicoquímica, Sergio Livingstone 1007, Santiago, Chile*
[e]*Centro para el Desarrollo de la Nanociencia y la Nanotecnología, CEDENNA, Chile*

†The authors dedicate this article to their friend Prof. Maria Teresa Garland because of her recent retirement.

‡Electronic supplementary information (ESI) available: DFT-optimized bond distances for all the species. DFT-computed orbitals and TDDFT transitions. CCDC 1446679 for [Br(CO)$_3$Re(μ-3-chloro-6-(4-diphenylphosphinyl)butoxypyridazine)$_2$Re(CO)$_3$Br]. For ESI and crystallographic data in CIF or other electronic format see DOI: 10.1039/c6dt04158b

Introduction

Rhenium(I) tricarbonyl complexes, Re(CO)$_3$L, having *N,N*-bidentate ligands have attracted interest because of their luminescence properties,[1–3] which have been shown to depend strongly on the nature of the bidentate ligand.[4–7] Complexes having a *P,N*-bidentate ligand have attracted much less attention compared to the ones bearing *N,N*-diimine groups, although hybrid ligands have been widely used due to their potential applications in different areas, *i.e.* catalysis.[8–12] We have recently described the photophysical properties of the mononuclear complex [*P,N*-{(C_6H_5)$_2$(C_5H_4N)P}Re(CO)$_3$Br] (**RePNBr**) (Scheme 1),[13] which was characterized as a dual emitter.[14] In addition, dramatic changes in the photophysical behavior were found when a NH fragment is inserted between

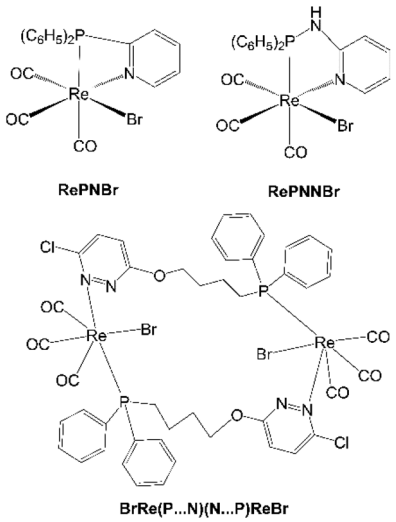

Scheme 1 Schematic structure of **RePNBr**, **RePNNBr**, and **BrRe(P···N)(N···P)ReBr**.

the P–N bond in the 2-(diphenylphosphino)pyridine ligand (*i.e.* [{$(C_6H_5)_2(C_5H_4N)NHP$}$Re(CO)_3Br$], **RePNNBr**, Scheme 1).[15]

The parent complex **RePNNBr** (Scheme 1) showed exclusively emission involving ligand centered transitions. In comparison to mononuclear complexes, binuclear complexes of hybrid ligands are even more scarce.[16]

In the present work we discuss the molecular and electronic structures of the new bimetallic complex $[Br(CO)_3Re(\mu$-3-chloro-6-(4-diphenylphosphinyl)butoxypyridazine$)_2Re(CO)_3Br]$ (**BrRe(P···N) (N···P)ReBr**) (Scheme 1), characterized by means of photophysical and X-ray diffraction measurements, cyclic voltammetry determinations and DFT/TDDFT calculations. Luminescence lifetimes and emission quantum yields are reported. The effect of the temperature on the stability of the complex is determined. The results are discussed in terms of the molecular and electronic structure of the compound and also in comparison with the behavior of mononuclear analogues **RePNBr** [13] and **RePNNBr**.[15]

Experimental

All reagents, $(Re(CO)_3(THF)Br)_2$ (THF: tetrahydrofuran), lithium diphenylphosphide solution and 3,6-dichloropyridazine, were used as received from the supplier (Aldrich). Solvents for synthesis were dried and freshly distilled before use. Standard Schlenk techniques were used for all solvent manipulations. Solvents for spectroscopic measurements: dichloromethane (DCM, HPLC grade, Merck), chloroform ($CHCl_3$, Analysis grade, EMSURE® Merck), acetonitrile (MeCN, HPLC grade, Merck), ethanol (EtOH, absolute grade, Merck), *N*,*N*-dimethylformamide (DMF, spectroscopic grade, Uvasol® Merck), methanol (MeOH, spectroscopic grade, Uvasol® Merck), and benzene (C_6H_6, analysis grade, EMSURE® Merck) were used as received. Argon (Ar, 99.99%, air liquid).

Synthesis

3-Chloro-6-(4-diphenylphosphinyl)butoxypyridazine (P···N). The ligand was obtained as the main product of the stoichiometric reaction of the lithium diphenylphosphide solution (100 mL, 0.5 mol L^{-1}, Aldrich) with 3,6-dichloropyridazine (3.724 g, 0.025 mol, Aldrich) in boiling THF for 3 h (Scheme 2), as previously described for the preparation of 3,6-bis(diphenylphosphinyl)pyridazine.[17] After filtration, the solvent was removed at low pressure, to give a colorless solid (yield 5.96 g, 78.0%).

Elemental analysis. The calculated (experimental) values for $C_{20}H_{20}N_2OClP$ are: C, 64.70 (66.60); H, 5.45 (6.06); N, 7.55 (7.27). ^{1}H NMR (400 MHz, $CDCl_3$) δ 7.33 (m, 10H), 6.82 (d, J = 9.2 Hz, 2H), 4.41 (d, J = 33.0 Hz, 2H), 2.04 (dd, J = 14.2, 6.0 Hz, 2H), 1.93–1.84 (m, 2H), 1.59–1.51 (m, 2H). ^{13}C NMR (101 Hz, $CDCl_3$) δ 164.12 (s), 150.67 (s), 138.29 (s), 132.42 (s), 130.51 (s), 128.29 (s), 128.22 (s), 119.91 (s), 67.20 (s), 29.82 (s), 27.42 (s), 22.17 (s).

$[Br(CO)_3Re(P\cdots N)(N\cdots P)Re(CO)_3Br]$, BrRe(P···N)(N···P)ReBr. The binuclear complex was obtained by the direct reaction of the **P···N** ligand (0.504 g, 1.125 mmol) with a $(Re(CO)_3(THF)Br)_2$ dimer (0.951 g, 1.125 mmol) in 100 mL of $CHCl_3$ at room temperature, as shown in Scheme 3. After stirring for 15 h, the solvent was removed at reduced pressure to give an orange solid. Yield, 1.202 g (93.2%). Crystallization from a DCM solution was achieved by slow evaporation.

Elemental analysis. The calculated[18] (experimental) values for **[BrRe(P···N)(N···P)ReBr]**·$(CHCl_3)$, are: C, 36.2 (36.2); H, 2.65 (2.78); N, 3.59 (3.01) %. ^{1}H NMR (400 MHz, $CDCl_3$) δ 7.71–7.27 (m, 10H), 3.75 (t, J = 6.3 Hz, 4H), 1.88–1.82 (m, 2H), 1.61 (s, 2H), 1.26 (s, 2H). ^{13}C NMR (101 MHz, $CDCl_3$) δ 133.79 (s), 131.44 (s), 129.21–129.01 (m), 68.59 (s), 26.22 (s). IR: ν_{CO}: 2038, 2030 and 1920 cm^{-1}.

Photophysical measurements

UV-Vis spectra were recorded on an Agilent 8453 Diode-Array spectrophotometer in the range of 250–600 nm in aerated solutions of different organic solvents. Emission spectra were

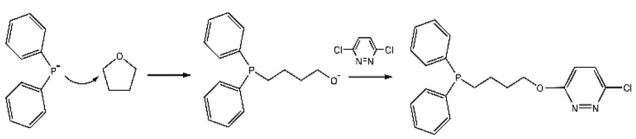

Scheme 2 Reaction leading to **P···N**.

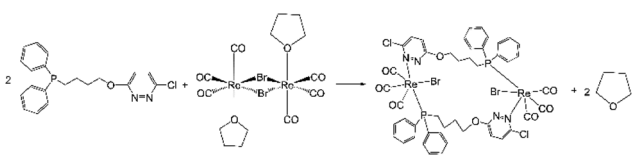

Scheme 3 Synthetic path to $[Br(CO)_3Re(P\cdots N)(N\cdots P)Re(CO)_3$ Br], **BrRe(P···N)(N···P)ReBr**.

recorded using a Horiba Jobin-Yvon FluoroMax-4 spectrofluorometer at room temperature. Experiments at 77 K were carried out in EtOH/MeOH glass (4 : 1, v/v). Complex emission spectra in the solid state were measured using a holder for solid samples at 45°. Emission quantum yields (Φ_{em}) were measured at room temperature using quinine sulfate in 0.1 M H_2SO_4 as an actinometer (Φ_{em} = 0.546 for excitation at 350 nm).[19] Luminescence lifetime measurements were carried out in a PicoQuant FluoTime 300 fluorescence lifetime spectrometer with a time correlated single photon counting technique. A LDH-P-C-405 laser was employed as the pulsed light source (FWHM ~54 ps; pulse energy 31 pJ). Singlet oxygen emission experiments were performed using the instrument "burst" mode, consisting of a train of laser pulses at a high (80 MHz) repetition rate (rather than a single pulse) and then switched off to detect the emission of the sample. The individual laser pulses act like a single long pulse with a much higher energy. The generation of singlet oxygen was monitored at 1270 nm using a Hamamatsu NIR-PMT detector (H10330-45). Quantum yields of singlet oxygen generation were measured at room temperature using perinaphthenone as an actinometer (Φ_Δ = 0.95 in DCM).[20] The experiments were carried out in either air-equilibrated or argon-saturated solutions. Nanosecond laser flash photolysis experiments were performed in argon saturated dichloromethane solutions by exciting at 355 nm and sweeping the absorption spectra between 400 and 640 nm. The instrument has been previously described.[21] Transient absorption data analysis was carried out using the program ASUFIT (available at http://www.public.asu.edu/laserweb/asufit/asufit.html). Kinetic traces over a selected wavelength region were globally fitted using the expression $\Delta A(\lambda,t) = \sum A_i(\lambda)\exp(-t/\tau_i)$ with i = 1,.., n; where $\Delta A(\lambda,t)$ is the observed absorption change at a given wavelength and time delay t and n is the number of kinetic components used in the fitting. A plot of $A_i(\lambda)$ *versus* wavelength is called a decay-associated spectrum (DAS), and represents the amplitude spectrum of the i^{th} kinetic component, which has a lifetime of τ_i.

Cyclic voltammetry

Cyclic voltammograms at room temperature for **BrRe(P···N)(N···P)ReBr** and **P···N** were recorded in DCM solutions (1.0 mM) using tetrabutylammonium perchlorate (0.10 M) as a supporting electrolyte. Cyclic voltammograms were recorded at 100 mV s^{-1} between +2.0 and −2.0 V. Before runs, the sample solutions were deoxygenated by bubbling nitrogen gas for 10 min. A vitreous carbon electrode was used as a working electrode, a platinum electrode as an auxiliary electrode, and an Ag/AgCl electrode as a reference electrode. Ferrocene was used as the internal standard ($E_{1/2}$ = 0.451 V; ΔE = 0.73 V).

X-ray diffraction

The crystal structure of the binuclear complex **BrRe(P···N)(N···P)ReBr** was determined by X-ray diffraction on a plate-shaped 0.105 × 0.083 × 0.029 mm^3 single crystal at 296 K. Data collection was done on a SMART CCD diffractometer using ϕ and ω-scans as collection strategies. Data were reduced using SAINT,[22] while the structure was solved by direct methods, completed by difference Fourier synthesis and refined by least-squares using SHELXL.[23] Multi-scan absorption corrections were applied using SADABS.[24] The occupancy of the solvent was refined and the convergence value was then held constant during the last refinement cycles. The hydrogen atom positions were calculated after each cycle of refinement using a riding model for each structure, with C–H distances ranging between 0.93 and 0.97 Å. U_{iso}(H) values were set equal to 1.2U_{eq} of the parent carbon atom. During the structure completion process by difference Fourier synthesis, it was clear that there were two partially occupied solvating chloroform sites present in the space left by the molecules of the complex within the cell, adding one molecule per dimer. Efforts to model the disorder of the solvating molecules by using a meaningful scheme partially failed, then we decided to use PLATON-SQUEEZE,[25,26] a well-documented method used for the modelling of unresolved electron density. Based on the elemental analysis, a molecule of chloroform per dimer was included into the final formula. Table S1 of the ESI‡ contains details of crystal and refinement parameters.

Computational details

All geometry optimizations were performed at the B3LYP/6-31+G(d′) level of theory using the Gaussian09 Rev C.01 package of programs (G09),[27] and started from the geometry determined by means of X-ray diffraction. The LANL2DZ basis set was used only for rhenium. Excited state calculations were performed within the time-dependent DFT methodology as implemented in G09 with B3LYP/6-31+G(d′,p′)/LANL2DZ. Solvent effects for simulating dichloromethane have been incorporated through the polarizable continuum model (PCM) using the integral equation formalism variant (IEFPCM).[28,29] Absorption and emission spectra were simulated from the above calculations using the GaussSum 3.0 suite of freely available processing tools. A full width at half-maximum (FWHM) of the Gaussian curves corresponding to 3000 cm^{-1} was employed to convolute both spectra. Representations for molecular orbitals were generated using the G09 cubegen tool and have been visualized using VMD and Pov-Ray 3.6 programs.[30,31]

Results and discussion

THF ring-opening to (P···N)

As commented on above in the Experimental section, under the experimental conditions, the reaction of lithium diphenylphosphide unexpectedly leads to the opening of the tetrahydrofuran ring and the formation of the ligand butoxypyridazine instead of simply producing the aromatic substitution product, 3,6-bis(diphenylphosphino)pyridazine. Considering the structure of the reactants and the resulting **P···N** ligand, it is clear that the THF ring-opening is induced by an attack of the diphenylphosphide on the carbon-2 of THF, resulting in the

formation of a reactive open-chain alkoxide intermediate, which subsequently attacks 3,6-dichloropyridazine to yield **P···N** (Scheme 2). In order to clarify the reason behind the ring opening compared to the direct attack on 3,6-dichloropyridazine,[17] it is important to emphasize that the same product is obtained when a lower temperature, 40 °C, and a longer reaction time are used. Examples of THF ring opening in reactions with either PPh_3 or NEt_3 can be found in the literature.[32,33] It has been previously reported that 3,6-dichloropyridazine leads to mono-substituted products when it reacts with bulky ligands, even if a 1 : 2 stoichiometry is used.[34,35] Differences would be tentatively attributed to the reaction mixing order and/or to the source of lithium diphenylphosphide.

Structural description

The determined structure of the **BrRe(P···N)(N···P)ReBr** complex corresponds to a bimetallic species having two $Re^{I}(CO)_3Br$ centres bridged by two 3-chloro-6-(4-diphenylphosphinyl)butoxypyridazine (**P···N**) molecules in a κ^2-*P*,*N* head to tail fashion, as shown in Fig. 1. Because of this coordination mode, the molecule has a crystallographic inversion centre and consequently, its molecular point group symmetry is C_i. The coordination geometry of each Re^{I} centre corresponds to a distorted octahedron with the three carbonyl groups in a *fac*-correlation. Similarly, for the mononuclear complexes **RePNBr** and **RePNNBr**, the phosphorus and nitrogen atoms display a *cis*-correlation, although for **BrRe(P···N)(N···P)ReBr** both belong to different ligand molecules. This is reflected in a "regular" value for the P1–Re1–N1 angle, 90.3(3)°, compared to 64.9(1)° and 78.0(2)° measured for **RePNBr**,[13,14] and **RePNNBr**,[15] where steric demand for chelation diminishes the angle. The compound has a cage structure, with 9.1470(15) Å between the two symmetry related Re^{I} centres (Table 1).

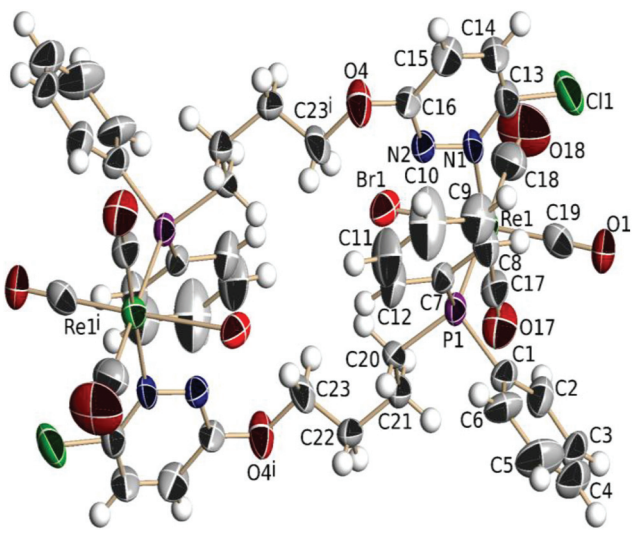

Fig. 1 Molecular structure plot for **BrRe(P···N)(N···P)ReBr**. Displacement ellipsoids are drawn at the 50% probability level, while H atoms are shown as spheres of arbitrary radii. Symmetry code: i: 2 − *x*, −*y*, 1 − *z*.

Table 1 Selected geometric parameters (Å, °) for **BrRe(P···N)(N···P)ReBr**

Re1–N1	2.213(10)	Re1–P1	2.491(3)
Re1–Br1	2.6442(13)	Re1–C17	1.865(11)
Re1–C19	1.858(13)	Re1–C18	1.996(19)
Re1···Re1^{i}	9.1467(14)		
N1–Re1–Br1	87.7(2)	P1–Re1–Br1	89.59(9)
N1–Re1–P1	90.3(3)		

Symmetry code: i: 2 − *x*, −*y*, 1 − *z*.

Cyclic voltammetry

To clearly understand the electrochemical behavior of the complex, we first characterized the (**P···N**) ligand. The molecule displays two irreversible processes, an oxidation wave with $E_{p,a}$ = +1.11 V (Fig. 2a, red line) and a reduction wave at $E_{p,c}$ = −1.84 V (Fig. 2b, red line). A comparison with literature values[36–38] suggests the participation of diphenylphosphine and pyridazine moieties in the oxidation and reduction processes, respectively.[39,40] The spin density determined by means of DFT over

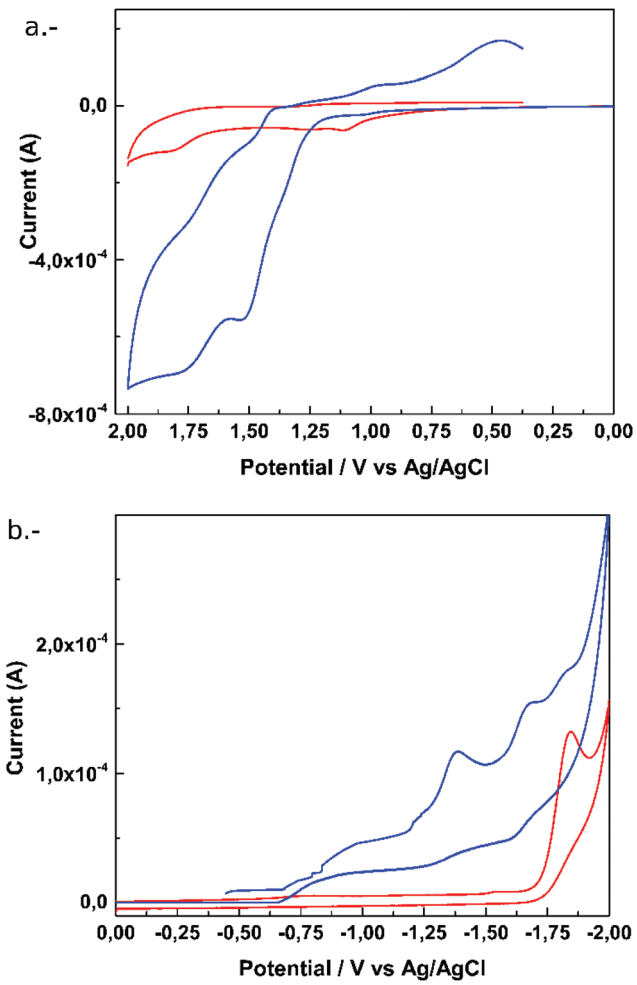

Fig. 2 Cyclic voltammograms for 3-chloro-6-(4-diphenylphosphinyl) butoxypyridazine, (**P···N**) (—) and **BrRe(P···N)(N···P)ReBr** (—). Anodic (a) and cathodic (b) potential scans.

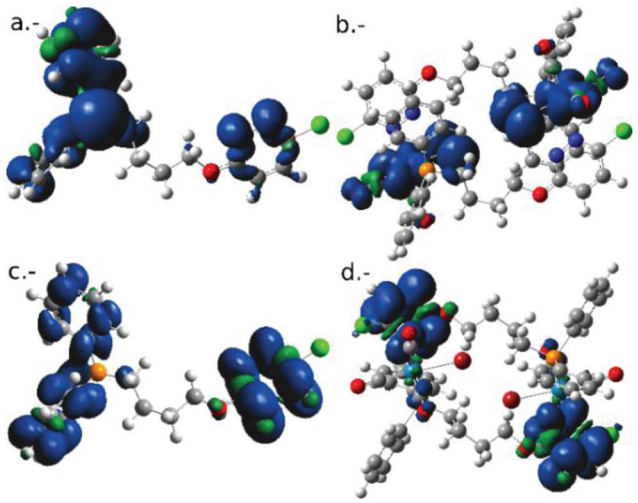

Fig. 3 Gas phase DFT computed spin density transitions for the oxidized species (a) **P···N**$^{\bullet+}$ and (b) **BrRe(P···N)(N···P)ReBr**$^{\bullet+}$ and the reduced species (c) **P···N**$^{\bullet-}$, and (d) **BrRe(P···N)(N···P)ReBr**$^{\bullet-}$.

the one-electron vertically oxidized and reduced forms of the molecule is completely consistent with this interpretation. Results shown in Fig. 3a and b suggest that the unpaired electron density is mainly distributed within the diphenyl and pyridazine fragments for **P···N**$^{\bullet+}$ and **P···N**$^{\bullet-}$, respectively.

For the compound **BrRe(P···N)(N···P)ReBr**, a positive scan starting at 0.0 V shows two consecutive oxidation processes, as shown in Fig. 2a and b (blue line). The first quasi-irreversible process occurs at $E_{p,a}$ = +1.50 V ($E_{1/2}$ = +1.46 V, ΔE_p = 130 mV) and the second irreversible one occurs at $E_{p,a}$ = +1.76 V. These processes may be assigned to metal-centered one-electron oxidations, Re^{I}/Re^{II} and Re^{II}/Re^{III}, which have been previously observed for rhenium(I) tricarbonyl complexes with multidentate nitrogen donor ligands [(*N*,*N*)Re(CO)$_3$X],[30,40] for the mononuclear compounds **RePNBr**[13] and **RePNNBr**,[15] and for [Re(1,2-bis(dimethylphosphino)ethane)$_3$].[41] In contrast, the cathodic scan for the dinuclear compound shows three irreversible signals at E_p *ca.* −1.38 V, −1.68 V and −1.82 V.

The irreversible reduction observed at E_p = −1.38 V is assigned to the Re^{I}/Re^{0} process.[40,42] The irreversible reductions observed around −1.68 V and −1.82 V are assigned to the reduction of the pyrazine moiety, which has been previously observed for *N*,*N*-$Re^{I}(CO)_3$ complexes,[40–43] followed by a possible decomposition of the complex. A similar reduction has also been observed in Re^{I} complexes with other *P*,*N*-ligands.[41] The corresponding values for **RePNBr** and **RePNNBr** are −1.20 and −1.75 V.[14,15] The absence of potential signals associated with the diphenylphosphine oxidation process ($E_{p,a}$ = +1.11 V) and pyridazine reduction process ($E_{p,c}$ = −1.82 V) should be related to electronic density differences between the free or coordinated ligand.[44] The DFT computed spin density for the one-electron vertically oxidized and reduced species **BrRe(P···N)(N···P)ReBr**$^{\bullet+}$ and **BrRe(P···N)(N···P)ReBr**$^{\bullet-}$, is consistent with oxidation centered on the metal and reduction centered on the ligand, specifically in the pyridazine fragment. Cyclic voltammetry results are summarized in Table 2.

Table 2 Anodic and cathodic peak potentials for **BrRe(P···N)(N···P)ReBr** and **P···N**. Potentials are reported in volts referred to the Fc^{+}/Fc couple

	$E_{p,a}$	$E_{p,a}$	$E_{p,c}$	$E_{p,c}$	$E_{p,c}$
BrRe(P···N)(N···P)ReBr	1.76	1.50	−1.38	−1.68	−1.82
P···N	1.11		−1.84		

DFT and TD-DFT results

In order to gain some insight into the electronic structure of the **P···N** ligand and the **BrRe(P···N)(N···P)ReBr** complex and their relation with the electronic spectra, we ran geometry optimizations on both compounds and calculated their excitations. The results are summarized in Table 3. Fig. 4 and S1‡ show the DFT computed frontier and near frontier orbitals involved in relevant UV-Vis excitations. Fig. 5 shows the corresponding spectra associated with the excitations computed

Table 3 Summary of main energy (*E*), wavelength (λ) and oscillator strength (*f*) computed for observed transitions in the absorption spectra of **P···N** and **BrRe(P···N)(N···P)ReBr**, together with the orbitals implicated in each transition, both in the gas phase

N	*E*/eV	λ/nm	*f*	Major contributions
P···N				
1	3.78	328	0.0036	HOMO−1 → LUMO (99%)
3	4.44	279	0.0457	HOMO−1 → LUMO+1 (71%)
4	4.587	271	0.0310	HOMO−3 → LUMO+1 (87%)
5	4.73	262	0.0609	HOMO → LUMO+3 (55%)
BrRe(P···N)(N···P)ReBr				
4	2.65	469	0.0286	HOMO−3 → LUMO (48%)
				HOMO−2 → LUMO+1 (47%)
10	3.29	377	0.1081	HOMO−5 → LUMO+1 (47%)
				HOMO−4 → LUMO (46%)
12	3.54	350	0.0257	HOMO−7 → LUMO (30%)
				HOMO−6 → LUMO+1 (34%)

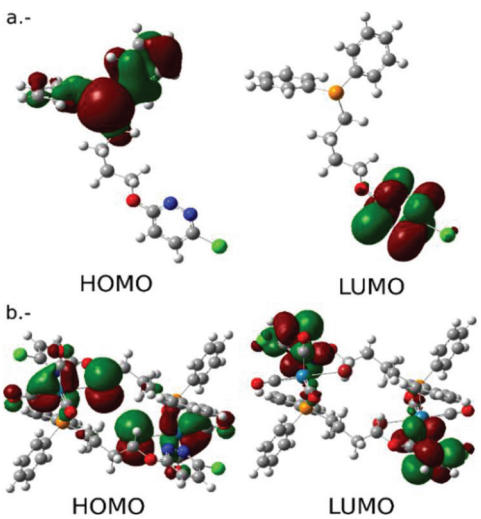

Fig. 4 DFT computed frontier orbitals for (a) **P···N** and (b) **BrRe(P···N)(N···P)ReBr**.

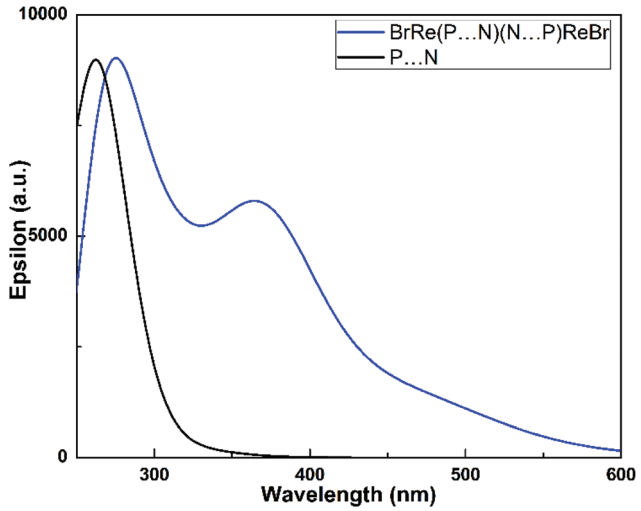

Fig. 5 TD-DFT computed spectra for **P···N** (—) and **BrRe(P···N)(N···P)ReBr** (—), both in the gas phase.

from TD-DFT. The combined results of Fig. S1‡ and Table 3 indicate that the absorption in the UV-Vis region for **BrRe(P···N)(N···P)ReBr** corresponds to a transition between a metal d-type orbital to a ligand-centered pyrazine π* orbital, MLCT.

Absorption spectra

Fig. 6a shows the absorption spectra of the ligand, **P···N**, and the complex, **BrRe(P···N)(N···P)ReBr**, both measured in DCM solution. The absorption spectrum of **P···N** exhibits two maxima at 231 nm ($\varepsilon = 1 \times 10^4$ M^{-1} cm^{-1}, not shown in Fig. 6) and 255 nm ($\varepsilon = 8 \times 10^3$ M^{-1} cm^{-1}). Their high molar absorptivities suggest that they correspond to ππ* transitions, the proposal being consistent with DFT results shown in Table 3. Moreover, TDDFT results (Fig. 5 and S1a† and Table 3) suggest that the main transition involved in these absorption bands corresponds to an intra-ligand ππ* excitation on the diphenylphosphinyl moiety. The complex, **BrRe(P···N)(N···P)ReBr**, presents similar bands and molar absorptivity values at a higher energy (265 nm, $\varepsilon = 2 \times 10^4$ M^{-1} cm^{-1}), however a new and broad band is observed at 380 nm ($\varepsilon = 7 \times 10^3$ M^{-1} cm^{-1}). By simple comparison to what was previously described for **P···N**, the band around 265 nm is assigned to a ππ* transition centered in the diphenylphosphinyl moiety. In contrast, the band centered around 380 nm is consistent with a MLCT transition, from a Re d-type orbital with the contribution of carbonyl groups ($Re_{d\pi}$) to a ligand π* orbital.[14] These assignments are highly consistent with the TDDFT results shown in Fig. 5 and S1b† and Table 3.

The inset in Fig. 6a shows the comparison with the absorption spectrum of **RePNBr**. For this monometallic Re^I complex, the MLCT band at 310 nm ($\varepsilon = 5 \times 10^3$ M^{-1} cm^{-1})[13,14] is blue-shifted as compared to that of **BrRe(P···N)(N···P)ReBr**. The lower energy of the MLCT absorption band for **BrRe(P···N)(N···P)ReBr** can be attributed to the different coordination of phosphorus and nitrogen atoms to the metallic center. In this case, the nitrogen atom from the pyridazine ring appears to

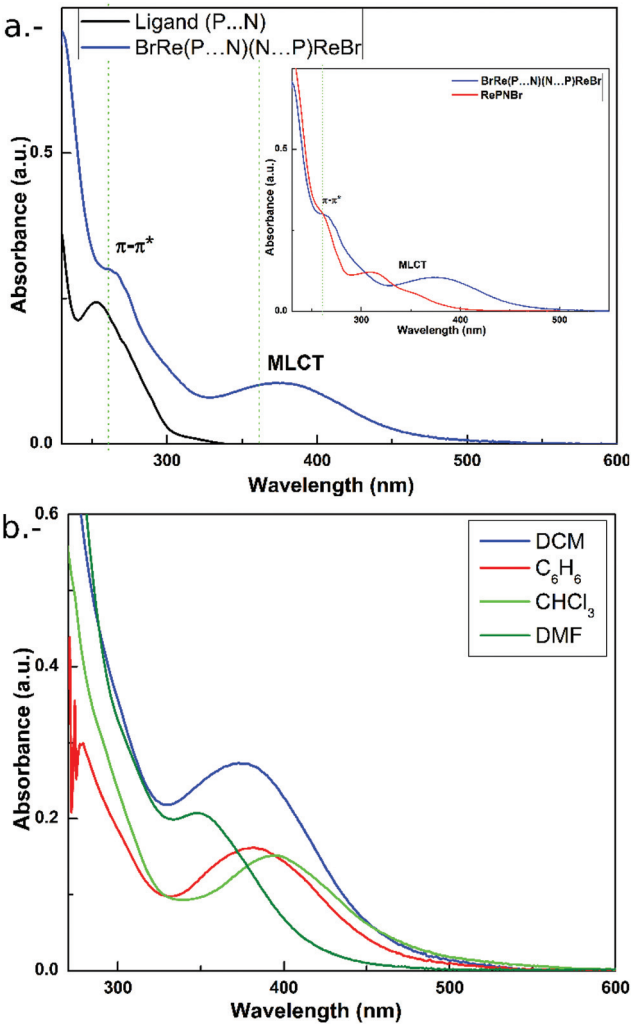

Fig. 6 (a) Absorption spectra of **P···N** (black) and **BrRe(P···N)(N···P)ReBr** (blue) in DCM solution. Inset: Comparison of absorption spectra of **BrRe(P···N)(N···P)ReBr** (blue) and **RePNBr** (red). (b) Solvent effect on the absorption spectra of **BrRe(P···N)(N···P)ReBr**.

have a major contribution (retro back donation effect) compared to the nitrogen of the pyridine ring, which is more restricted due to its binding to the diphenylphosphinyl group. On the other hand, Fig. 6b shows the typical solvent effect observed for MLCT absorption bands. Except for the spectrum in benzene, which shows anomalous behavior presumably due to the significant polarizability of the benzene ring delocalized π orbital,[45,46] a successive hypsochromic shift is observed with increasing solvent polarity. This negative solvatochromism is associated with a reduced and reversed molecular dipole in the MLCT state relative to that of the ground state.[1,45,47–50]

Decomposition in solution

During the photophysical experiments in solution, a noticeable absorption decrease was detected in most of the essayed solvents, then a decomposition study was done for the complex in acetonitrile, where the effect was found to be more

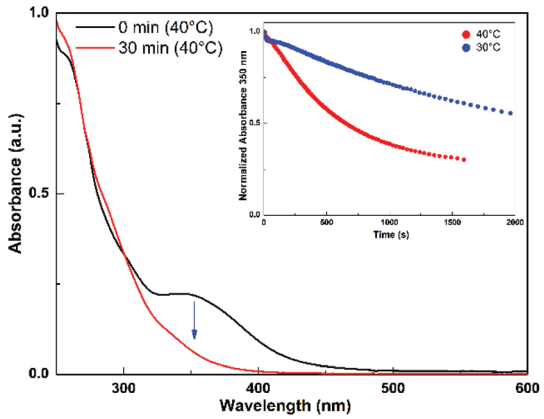

Fig. 7 Absorption spectra of **BrRe(P···N)(N···P)ReBr** in MeCN at 40 °C at different times: 0 min (black) and 20 min (red). Inset: Normalized absorbance decay at 350 nm.

pronounced, as normally expected for coordinating solvents, which may replace a weakly coordinated ligand in the Re^{I} environment, as described by Mella *et al.*[51] (and references therein), and favor decomposition. In this solvent, the MLCT absorption band (at 350 nm) decreased its intensity following first order kinetics as can be seen in Fig. 7. The consumption rate constant, which we assign to a ligand exchange, depends on the temperature, as shown in the inset in Fig. 7. An Arrhenius activation energy of 21 kcal mol^{-1}, from the measurements at four different temperatures, was estimated for the ligand exchange process in MeCN solution.

Emission properties

At room temperature, a weak emission is observed upon the excitation of **BrRe(P···N)(N···P)ReBr** at any of its previously described absorption maxima, 265 nm or 375 nm. As shown in Fig. 8a and Table 4, the emission decay follows a biexponential law with two luminescence lifetimes, τ_1 = 24 ns, and τ_2 = 4.7 ns. Similar low quantum yields and lifetime values were observed for complex **RePNBr**, which has been previously described as a dual emissor.[14] Then, the possibility of having two emissive states was explored with Time-Resolved Emission Spectra (TRES) experiments. Emissions from impurities or decomposition products were discarded using the recrystallized compound and freshly prepared solutions every time. The inset in Fig. 8a shows that the transition associated with each lifetime has a different peak energy. The shortest lifetime with a higher amplitude has a maximum at a higher energy (480 nm) as compared to the longest lifetime which shows a band with the maximum at 600 nm. On the other hand, at 77 K in a solid matrix, an intense, broad and unstructured emission band with the maximum at 535 nm can be observed when the complex is excited at 375 nm (MLCT transition, Fig. 8b). In the solid state (powder) at room temperature, the complex shows a red-shifted emission centered at 570 nm. A triplet character could be attributed to this MLCT excited state because as can be seen from Fig. 8c, the emission centered at

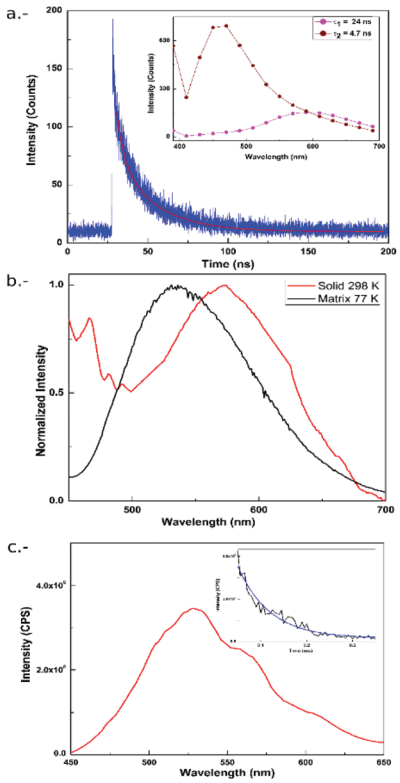

Fig. 8 (a) Biexponential emission decay of **BrRe(P···N)(N···P)ReBr** measured in DCM at 580 nm. Data recorded at room temperature. Inset: Time resolved emission spectrum of the complex. (b) Emission spectrum of **BrRe(P···N)(N···P)ReBr** in solid at 278 K (red line), and solid matrix (EtOH/MeOH, 4 : 1) at 77 K (black line). (c) Delayed luminescence of **BrRe(P···N)(N···P)ReBr** after 50 μs in EtOH/MeOH (4 : 1) at 77 K. Inset: Delayed luminescence decay at 540 nm. Excitation wavelength for every experiment: 375 nm.

Table 4 Summary of the photophysical properties of **BrRe(P···N)(N···P)ReBr** in air equilibrated DCM solution[a]

Solvent	λ_{abs}/nm ($\varepsilon/10^3$ M^{-1} cm^{-1})	λ_{em}/nm	Φ_{em}	τ[b]/ns	Φ_{Δ}
DCM	265 (20) 380 (7.0)	580	$<1 \times 10^{-3}$	24 (61%); 4.7 (39%)	0.045

[a] Errors were lower than 10%. [b] Values in parentheses are amplitudes in percent contribution from each decay component.

540 nm has a long lifetime, in the order of 69.7 μs, characteristic of a forbidden triplet → singlet transition. Furthermore, it was possible to detect singlet oxygen generation by the complex in DCM solution upon excitation at 375 nm, which is usually associated with the presence of a species with a triplet excited state character.[52]

Dual emission for **RePNBr** was hypothesized to come from two states very close in energy associated with π^*_{phenyl} and $\pi^*_{pyridil}$.[14] Although **BrRe(P···N)(N···P)ReBr** has a higher number of metal centers, it preserves the dual emitting nature when compared to its closely related precursor **RePNBr**. This behavior seems to occur

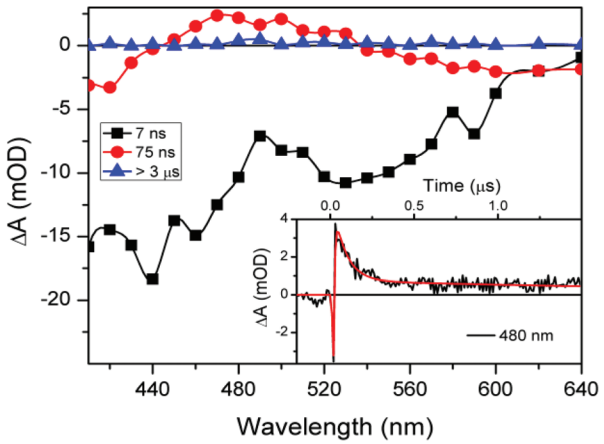

Fig. 9 Transient absorption DAS of **BrRe(P···N)(N···P)ReBr** measured in argon saturated DCM. Inset: Kinetic trace measured at 480 nm (black trace) and the corresponding fit (red line).

even if the phenyl and the pyridazine rings coordinated to each Re^{I} center do not belong to the same ligand molecule. By comparison, the dual emitting nature of **BrRe(P···N)(N···P)ReBr** could be explained to be coming from π^*_{phenyl} and $\pi^*_{pyridazine}$, which is also consistent with the results computed from DFT/TDDFT (Fig. S1b‡ and Table 3). For the case of **RePNNBr**, no emission from the ^{3}MLCT excited state was observed.[15]

Transient absorption

To further explore the excited state kinetics of **BrRe(P···N)(N···P)ReBr** we performed flash photolysis experiments in argon saturated DCM. A satisfactory global fit to the data was achieved using three exponential components; 7 ns, 75 ns and >3 μs, see Fig. 9. The shortest component, being on the order of the laser pulse duration, cannot be reliably resolved and was constrained to be less than 10 ns. This component is associated with the short lived emissive state observed in TRES experiments; it shows negative amplitudes from 400 to 640 nm (black line Fig. 9) consistent with a combination of ground state absorption recovery (400–510 nm) and stimulated emission decay (400–640 nm). The 75 ns component is associated with the long lived emissive state observed in TRES experiments (25 ns in air equilibrated DCM); it shows negative amplitudes from 400 to 440 nm and from 540 to 640 nm (red line Fig. 9) consistent with a combination of ground state absorption recovery (400–510 nm) and stimulated emission decay (500–700 nm). The positive amplitude signal centered around ~490 nm is assigned to the transient absorption decay of the long lived emissive state in analogy to the previously published results for **RePNBr**.[14] The long component (blue line Fig. 9) does not decay in the measured timescale (see insert) and shows very small positive amplitudes over the whole range; it can be assigned to a photoproduct based on a small amount (>10%) of permanent ground state absorption bleaching observed after the experiments. No transient state was observed when the solution was equilibrated with air suggesting that the observed signals in Ar saturated solutions correspond to states with triplet multiplicity (completely quenched in the presence of oxygen).

Conclusions

The results obtained confirm that under our experimental conditions lithium diphenylphosphide attacks THF, leading to 3-chloro-6-(4-diphenylphosphinyl)butoxypyridazine (**P···N**). The reaction of this ligand with the $(Re(CO)_3(THF)Br)_2$ dimer generates the [$Br(CO)_3Re$(μ-3-chloro-6-(4-diphenylphosphinyl) butoxypyridazine)$_2Re(CO)_3Br$] complex (**BrRe(P···N) (N···P)ReBr**) in high yield at room temperature. Experimental results indicate that the lowest energy UV-vis absorption maxima (occurring at 380 nm in DCM) have a MLCT character. The weak emission observed for **BrRe(P···N)(N···P)ReBr** at room temperature implies that non-radiative deactivation pathways are favored over radiative decay. This can be mainly attributed to the conformational flexibility of **P···N**'s long carbon chain, which provides efficient electronic-to-vibrational coupling modes for non-radiative deactivation in the complex, the same underlying reason behind the limited thermal stability of the compound in solution. Lowering the temperature to 77 K hinders vibrational deactivation, allowing the observation of an intense emission associated with a triplet MLCT excited state. At room temperature, the luminescence decays with two lifetimes τ_1 of 24 ns and τ_2 of 4.7 ns. This feature indicates that despite its higher number of metal centers, **BrRe(P···N)(N···P)ReBr** preserves the dual emitting nature previously reported for the homologous mononuclear complex **RePNBr**. DFT/TDDFT results for **BrRe(P···N)(N···P)ReBr** indicate that two MLCT states with significant contribution of π^*_{phenyl} and $\pi^*_{pyridazine}$ orbitals are responsible for the observed biexponential emission decay.

Acknowledgements

The authors gratefully acknowledge partial financial support from Comisión Nacional de Investigación Científica y Tecnológica, grants FONDECYT 1160546, 1160749 and ACT-1404 and Financiamiento Basal para Centros Científicos y Tecnológicos de Excelencia FB0807. The authors thank PicoQuant for support provided to purchase the FluoTime 300 system currently operating at UNAB. This work has been supported in part by grants from ANPCyT, Argentina (PICT 214/14); CONICET, Argentina (PIP 11220150100295/2015) and the Secretaría de Ciencia y Técnica, UNRC (PPI 2016) Argentina. M. L. G. and R. E. P. are permanent research staff of CONICET.

Notes and references

1 A. Kumar, S.-S. Sun and A. J. Lees, in *Photophysics of Organometallics*, ed. J. A. Lees, Springer Berlin Heidelberg, Berlin, Heidelberg, 2010, pp. 37–71, DOI: 10.1007/3418_2009_2.

2 A. Vlček, in *Photophysics of Organometallics*, ed. J. A. Lees, Springer Berlin Heidelberg, Berlin, Heidelberg, 2010, pp. 115–158, DOI: 10.1007/3418_2009_4.
3 E. Baggaley, J. A. Weinstein and J. A. G. Williams, *Coord. Chem. Rev.*, 2012, **256**, 1762–1785.
4 H. C. Bertrand, S. Clède, R. Guillot, F. Lambert and C. Policar, *Inorg. Chem.*, 2014, **53**, 6204–6223.
5 P. Kurz, B. Probst, B. Spingler and R. Alberto, *Eur. J. Inorg. Chem.*, 2006, 2966–2974, DOI: 10.1002/ejic.200600166.
6 A. P. Zipp, L. Sacksteder, J. Streich, A. Cook, J. N. Demas and B. A. DeGraff, *Inorg. Chem.*, 1993, **32**, 5629–5632.
7 L. Wallace and D. P. Rillema, *Inorg. Chem.*, 1993, **32**, 3836–3843.
8 B. Machura, A. Jankowska, R. Kruszynski, J. Kłak and J. Mroziński, *Polyhedron*, 2006, **25**, 2663–2672.
9 B. Machura and R. Kruszynski, *Polyhedron*, 2006, **25**, 1985–1993.
10 B. Machura and R. Kruszynski, *J. Mol. Struct.*, 2007, **837**, 92–100.
11 A. Pfaltz and W. J. Drury, *Proc. Natl. Acad. Sci. U. S. A.*, 2004, **101**, 5723–5726.
12 Z.-Z. Zhang and H. Cheng, *Coord. Chem. Rev.*, 1996, **147**, 1–39.
13 F. Venegas, N. Pizarro and A. Vega, *J. Chil. Chem. Soc.*, 2011, **56**, 823–826.
14 N. Pizarro, M. Duque, E. Chamorro, S. Nonell, J. Manzur, J. R. de la Fuente, G. Gunther, M. Cepeda-Plaza and A. Vega, *J. Phys. Chem. A*, 2015, **119**, 3929–3935.
15 P. Mella, J. C. Palma, M. Cepeda-Plaza, P. Aguirre, J. Manzur, G. Günther, N. Pizarro and A. Vega, *Polyhedron*, 2016, **111**, 64–70.
16 L. R. Pignotti, R. L. Luck, N. Deligonul, J. D. Protasiewicz, K. E. Johnson, L. P. Nguyen and E. Urnezius, *Inorg. Chim. Acta*, 2015, **424**, 274–285.
17 Z.-Z. Zhang, H.-K. Wang, Y.-J. Shen, H.-G. Wang and R.-J. Wang, *J. Organomet. Chem.*, 1990, **381**, 45–52.
18 L. Patiny and A. Borel, *J. Chem. Inf. Model.*, 2013, **53**, 1223–1228.
19 G. A. Crosby and J. N. Demas, *J. Phys. Chem.*, 1971, **75**, 991–1024.
20 F. Wilkinson, W. P. Helman and A. B. Ross, *J. Phys. Chem. Ref. Data*, 1993, **22**, 113–262.
21 C. Solis, J. J. Torres, N. Gsponer, C. Previtali, R. Palacios, H. Montejano and C. Chesta, *Photochem. Photobiol. Sci.*, 2013, **12**, 2146–2159.
22 *M. SAINTPLUS V6.22*, Bruker AXS Inc., WI, USA.
23 G. M. Sheldrick, *SHELXL97*, 1997.
24 *W. SADABS V2.05*, Bruker AXS Inc., Madison, USA.
25 A. L. Spek, *Acta Crystallogr., Sect. C: Cryst. Struct. Commun.*, 2015, **71**, 9–18.
26 P. van der Sluis and A. L. Spek, *Acta Crystallogr., Sect. A: Fundam. Crystallogr.*, 1990, **46**, 194–201.
27 M. J. T. Frisch, G. W. Schlegel, H. B. Scuseria, G. E. Robb, M. A. Cheeseman, J. R. Scalmani, G. Barone, V. Mennucci, B. Petersson, G. A. Nakatsuji, H. Caricato, M. Li, X. Hratchian, H. P. Izmaylov, A. F. Bloino, J. Zheng, G. Sonnenberg, J. L. Hada, M. Ehara, M. Toyota, K. Fukuda, R. Hasegawa, J. Ishida, M. Nakajima, T. Honda, Y. Kitao, O. Nakai, H. Vreven, T. Montgomery, J. A. Peralta Jr., J. E. Ogliaro, F. Bearpark, M. Heyd, J. J. Brothers, E. Kudin, K. N. Staroverov, V. N. Kobayashi, R. Normand, J. Raghavachari, K. Rendell, A. Burant, J. C. Iyengar, S. S. Tomasi, J. Cossi, M. Rega, N. Millam, N. J. Klene, M. Knox, J. E. Cross, J. B. Bakken, V. Adamo, C. Jaramillo, J. Gomperts, R. Stratmann, R. E. Yazyev, O. Austin, A. J. Cammi, R. Pomelli, C. Ochterski, J. W. Martin, R. L. Morokuma, K. Zakrzewski, V. G. Voth, G. A. Salvador, P. Dannenberg, J. J. Dapprich, S. Daniels, A. D. Farkas, Ö. Foresman, J. B. Ortiz, J. V. Cioslowski and D. J. Fox, vol. Revision D.01, Gaussian, Inc., Wallingford CT, 2009.
28 S. Miertuš, E. Scrocco and J. Tomasi, *Chem. Phys.*, 1981, **55**, 117–129.
29 S. Miertuš and J. Tomasi, *Chem. Phys.*, 1982, **65**, 239–245.
30 K. Potgieter, P. Mayer, T. Gerber, N. Yumata, E. Hosten, I. Booysen, R. Betz, M. Ismail and B. van Brecht, *Polyhedron*, 2013, **49**, 67–73.
31 W. Humphrey, A. Dalke and K. Schulten, *J. Mol. Graphics*, 1996, **14**, 33–38.
32 G. C. Welch, J. D. Masuda and D. W. Stephan, *Inorg. Chem.*, 2006, **45**, 478–480.
33 S. M. Kunnari, R. Oilunkaniemi, R. S. Laitinen and M. Ahlgren, *J. Chem. Soc., Dalton Trans.*, 2001, 3417–3418, DOI: 10.1039/B108790H.
34 M. H. Sherif, G. A. Ahmed, A. A. Elbahnasawy and E. O. Helal, *J. Am. Sci.*, 2010, **6**, 570–574.
35 N. M. Abd El-Salam, Z. Y. Al Shoaibi and G. A. Ahmed, *Eur. J. Chem.*, 2011, **8**, 1944–1950.
36 C. C. Ko, A. W. Y. Cheung and S. M. Yiu, *Polyhedron*, 2015, **86**, 17–23.
37 J. J. Cid, J. Mohanraj, M. Mohankumar, M. Holler, F. Monti, G. Accorsi, L. Karmazin-Brelot, I. Nierengarten, J. M. Malicka, M. Cocchi, B. Delavaux-Nicot, N. Armaroli and J. F. Nierengarten, *Polyhedron*, 2014, **82**, 158–172.
38 J. R. Dilworth, P. Jobanputra, J. R. Miller, S. J. Parrott, Q. Chen and J. Zubieta, *Polyhedron*, 1993, **12**, 513–522.
39 D. Pandiarajan and R. Ramesh, *Polyhedron*, 2012, **34**, 136–142.
40 M. Panigati, M. Mauro, D. Donghi, P. Mercandelli, P. Mussini, L. De Cola and G. D'Alfonso, *Coord. Chem. Rev.*, 2012, **256**, 1621–1643.
41 J. R. Kirchhoff, M. R. Allen, B. V. Cheesman, O. Ken-ichi, W. R. Heineman and E. Deutsch, *Inorg. Chim. Acta*, 1997, **262**, 195–202.
42 G.-F. Wang, Y.-Z. Liu, X.-T. Chen, Y.-X. Zheng and Z.-L. Xue, *Inorg. Chim. Acta*, 2013, **394**, 488–493.
43 S. A. Moya, J. Guerrero, R. Pastene, R. Sartori, R. Schmidt, R. Sariego, J. Sanz-Aparicio, I. Fonseca and M. Martinez-Ripoll, *Inorg. Chem.*, 1994, **33**, 2341–2346.
44 A. Raimondi, M. Panigati, D. Maggioni, L. D'Alfonso, P. Mercandelli, P. Mussini and G. D'Alfonso, *Inorg. Chem.*, 2012, **51**, 2966–2975.

45 J. R. Lakowicz, *Principles of fluorescence spectroscopy*, Springer, New York, 2006.
46 R. E. Palacios, G. Kodis, C. Herrero, E. M. Ochoa, M. Gervaldo, S. L. Gould, J. T. M. Kennis, D. Gust, T. A. Moore and A. L. Moore, *J. Phys. Chem. B*, 2006, **110**, 25411–25420.
47 M. Wrighton and D. L. Morse, *J. Am. Chem. Soc.*, 1974, **96**, 998–1003.
48 G. Geoggroy and M. S. Wrighton, *Organometallic Photochemistry*, Academic Press, Inc, New York, 1979.
49 J. A. McCleverty and T. J. Meyer, *Comprehensive coordination chemistry II: from biology to nanotechnology*, Elsevier Pergamon, 2004.
50 D. J. Stufkens, *Comments Inorg. Chem.*, 1992, **13**, 359–385.
51 P. Mella, K. Cabezas, C. Cerda, M. Cepeda-Plaza, G. Gunther, N. Pizarro and A. Vega, *New J. Chem.*, 2016, **40**, 6451–6459.
52 F. Wilkinson, D. J. McGarvey and A. F. Olea, *J. Am. Chem. Soc.*, 1993, **115**, 12144–12151.